Aeroacoustic Optimization of Wind Turbine Blades

Simão Santos Rodrigues
simao.rodrigues@ist.utl.pt

Instituto Superior Técnico, Lisboa, Portugal

November 2012

Abstract

Power production from wind energy has been increasing for the past few decades, with more areas being used as wind farms and larger wind turbines being built. With this development, awareness of the impact of wind energy on the environment and on human health has also increased. Much research has been done to predict and reduce the noise generated by wind turbines. In this work, a blade element momentum theory model is used to predict the aerodynamic performance of a wind turbine, coupled to an empirical aeroacoustic noise model based on the works of Brooks et al [2] and Amiet [1], and using the XFOIL [6] panel code for the boundary layer computations. The aeroacoustic prediction code developed was validated against measurement data of the NREL Phase II and AOC 15/50 wind turbines and used in the optimization framework pyOpt, using the genetic algorithm NSGA-II [5]. The geometry of the blade was parameterized using NURBS curves for the cross sectional airfoil shapes and Bezier curves for the twist and chord distributions. Various optimizations were performed in blades of the two previous turbines, both single- and multi-objective, totaling up to 62 design variables. The optimal solutions are indicated in the obtained Pareto fronts and their geometries are discussed in detail. These solutions ranged from an increase in annual energy production of 139.9% to a reduction in noise levels of 10.7%. It was demonstrated that significant noise reduction could be obtained at an expense of a minor aerodynamic penalty.

Keywords: Genetic algorithms, NURBS, Multi-disciplinary design optimization, Multi-objective optimization

1. Introduction

For the past few decades, wind energy has seen a big development, with larger wind turbines (WT) being used and more wind farms being constructed. This increase led to an increase in awareness of the impacts of wind energy in the environment and human health, with many studies being performed on this subject [3]. While there are no common international noise standards or regulations for sound pressure levels, these are usually regulated by the legislation of each country, which defines maximum noise levels according to time of day and type of area. These limitations to generated noise make it necessary to address the issue in the design phase of wind turbines. The main objective of this work was to develop a framework to perform multi-disciplinary optimization of wind turbine blades, with respect to their aerodynamic and aeroacoustic performance. In order to do so, a bibliographic research on the subjects required for a complete understanding of the problem was performed. A wind turbine aerodynamic prediction model was implemented and later coupled to an aeroacoustic prediction model. A parameterization model of the geometry of a wind turbine blade was also developed. The final prediction code was integrated in an optimization framework, also developed in this work.

2. Theoretical Models

In this section, a theoretical background of the aerodynamic, aeroacoustic and parameterization models is presented and briefly discussed.

2.1. Aerodynamic Model

The aerodynamic model, besides predicting the aerodynamic performance of the wind turbine, provides the detailed results necessary for the aeroacoustic model, such as radial distribution of relative wind speed, Reynolds number and effective angle of attack. A Blade Element Momentum (BEM) theory model was implemented [9], with corrections for the hub- and tip-losses and turbulent wake state.

The airfoil data used in the BEM iterations can be corrected for 3D effects using the stall delay model from Du and Selig [7], with the drag adjustments from Eggers et al [8]. The data is extrapolated using a method developed by Viterna and Janetzke [16].

The Annual Energy Production (AEP) of the wind turbine is computed by assuming the proba-

bility density function of the wind to be a Weibull distribution, modeled through of a scaling factor A and a form factor k. The total annual energy production (AEP) can then be estimated as the product of the probability function and the power curve [9]

$$AEP = \sum_{i=1}^{N-1} \begin{array}{l} \frac{1}{2}\left(P\left(V_{i+1}\right) + P\left(V_i\right)\right) \\ \times f\left(V_i < V_0 < V_{i+1}\right) \\ \times 8760 \end{array}, \quad (1)$$

where $P\left(V_i\right)$ is the power produced by the wind turbine in a wind speed V_i, $f\left(V_i < V_0 < V_{i+1}\right)$ is the probability of the wind speed lying between V_i and V_{i+1} and the constant term refers to the number of hours existent in a year.

2.2. Aeroacoustic Model

The aeroacoustic prediction model developed in this work predicts both the turbulent inflow noise and the five mechanisms of the airfoil-self noise. [17]

Turbulent Inflow Noise The turbulent inflow noise is predicted using the model developed by Amiet [1] and modified by Lowson [12]. For the high frequencies, it yields

$$L_{p,inf}^{H} = 10\log_{10}\left(\frac{\rho^2 c_0^4 d}{2r_e^2} L I^2 \frac{M^5 \hat{k}^3 \bar{D}}{\left(1+\hat{k}^2\right)^{7/3}}\right) + 78.4, \quad (2)$$

where ρ is the density of air, c_0 is the speed of sound, d is the airfoil section span, L is the turbulence length scale, I is the intensity of turbulence, M is the Mach number, $\bar{D}$ denotes the effect from sound directivity, r_e is the distance from the observer and $\hat{k} = k/k_e$ is the wave number $k = 2\pi f/U$ normalized by the wave number range of energy-containing eddies $k_e = 3/4L$. U is the local inflow velocity. For the low frequencies, a correction factor is applied to the previous equation,

$$L_{p,\text{inflow}} = L_{p,\text{inf}}^{H} + 10\log_{10}\frac{K_c}{1+K_c}, \quad (3)$$

where K_c is a low frequency correction factor. This model, being based on experiments performed on a flat plate by Amiet, does not account for the geometry of the airfoil, thus a correction factor developed by Moriarty et al [13, 14] is applied to Eq. 3. The total turbulent inflow noise is then obtained with

$$L_{p,\text{airfoil}} = \Delta L_p + L_{p,\text{flat plate}} + 10, \quad (4)$$

where ΔL_p is the correction for the geometry of the airfoil and the term 10 is a correction to match with NRL data.

The turbulence parameters I is computed as function of the surface roughness z_0 and height z,

$$I = \gamma \frac{\ln\left(30/z_0\right)}{\ln\left(z/z_0\right)}, \quad (5)$$

where

$$\gamma = 0.24 + 0.096\log_{10} z_0 + 0.016(\log_{10} z_0)^2. \quad (6)$$

Airfoil Self-Noise Airfoil self noise is produced when an airfoil encounters a steady non turbulent flow field. It can be split into five mechanisms, as described by Brooks, Pope and Marcolini (BP&M) [2]:

1. Turbulent boundary layer trailing edge noise,
2. Separation-stall noise,
3. Laminar boundary layer vortex shedding noise,
4. Trailing edge bluntness vortex shedding noise,
5. Tip vortex formation noise.

The 1/3 octave noise spectrum produced by the first three mechanisms can be predicted by semi empirical scaling laws given by BP&M, in the form

$$L_{p,i} = 10\log_{10}\left(\frac{\delta_i M^{f(i)} L \bar{D}}{r_e^2}\right) + F_i\left(\text{St}\right) + G_i\left(\text{Re}\right), \quad (7)$$

where δ_i can be either the boundary layer thickness or displacement thickness, and $f(i)$ a value which depends on the noise mechanism. The terms $F_i\left(\text{St}\right)$ and $G_i\left(\text{Re}\right)$ are spectral shape functions based on the Strouhal number St and Reynolds number Re, respectively, which are different for each mechanism. Trailing edge bluntness vortex shedding and Tip vortex formation noises are also predicted in a similar way, with the first using spectral shape functions based on the trailing edge solid angle Ψ_{TE} and trailing edge thickness h.

WT Rotor Noise Prediction The total noise produced by the WT rotor is computed by dividing the blade in n elements. The two-dimensional noise prediction is performed for each element and the total sound pressure level generated by the rotor is the result of a summation of the noise from each blade element $L_{p,i}$,

$$L_{p,total} = 10\log_{10}\left(\frac{N_B}{N_{az}} \sum_i 10^{\frac{L_{p,i}}{10}}\right), \quad (8)$$

where N_{az} is the number of azimuthal positions at which the blade is computed and N_B is the number of blades. The Overall Sound Pressure Level

(OASPL) can be obtained by summing the noise levels at every frequency,

$$OASPL = 10\log_{10}\left(\sum_j 10^{\frac{L_{p,j}}{10}}\right), \qquad (9)$$

where $L_{p,j}$ is the total noise level at frequency j.

Boundary Layer Parameters The boundary layer parameters used in the noise prediction are computed at each element using the XFOIL [6] viscous-inviscid interactive code.

2.3. Geometry Parameterization Model

The geometry of the blade was parameterized by a set of control points defining the twist and chord distributions, which were either linearly interpolated or used to construct Bézier curves, and a set of control airfoil sections. After a survey on the most commonly used methods in airfoil shape parameterization, an approach using two NURBS curves, for the upper and lower sides of the airfoil, was chosen. The main advantages of this parameterization include the direct connection between the parameters and geometry, easy controllability of inflection points and local approximation.

Each of the two curves is defined by seven control points and a knot vector

$$\mathbf{U} = \left\{0, 0, 0, 0, \tfrac{1}{3}, \tfrac{1}{2}, \tfrac{2}{3}, 1, 1, 1, 1\right\}. \qquad (10)$$

The total number of available degrees of freedom of the control points is 20, as schematically represented in Fig. 1.

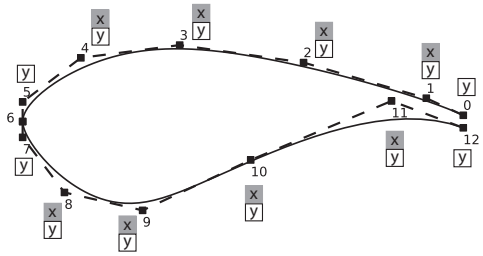

Figure 1: NURBS airfoil parameterization control points and respective degrees of freedom.

3. Implementation

In this section, a description of the developed prediction tool is presented, followed by a description of its implementation in a Multi-disciplinary Design Optimization (MDO) framework.

3.1. WT Aeroacoustic Prediction Tool

The aerodynamic, aeroacoustic and parameterization models described in the previous section were implemented in an prediction tool, using C++ and Python programming languages. The prediction tool is robust and flexible, allowing the configuration of the simulations in detail.

3.2. Optimization Framework

An MDO framework was implemented using the Python module pyOpt [15]. The chosen optimization algorithm was the genetic algorithm NSGA-II [5].

A convergence study was performed, in order to gain insight of the minimum population size and number or generations required to obtained a converged solution. The evolution of the fitness of the population of an optimization case with 8 design variables is presented in Fig. 2, where it can be seen that, with a population size of 8 individuals, the solution converges with much less function calls and the optimal solution produces an AEP value with a difference of about 1 % of the solution obtained with a population size of 64 individuals.

Based on this and other results, it was concluded that a population size between n and $2n$, with n being the number of design variables, is able to provide an accurate solution while maintaining the computational costs of the optimization low.

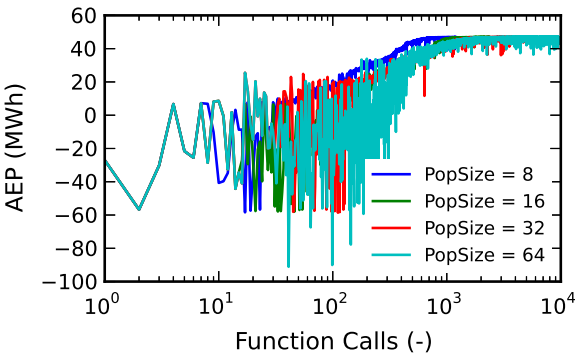

Figure 2: Evolution of the fitness of the population of an optimization case with 8 design variables (twist + chord).

3.3. Validation of the aeroacoustic prediction code

The AOC 15/50 wind turbine is a downwind three bladed wind turbine with a rated power of 50 kW. It uses the NREL S821, S819 and S820 profiles, defined at 40, 75 and 95 % of chord, respectively. The measured and predicted power curves are presented in Fig. 3, where slight overprediction can be observed up to a wind speed of approximately 14 $\mathrm{m\,s^{-1}}$. After that it slighly underpredicts the maximum power generated and fails to predict the loss in power due to stall.

In Fig. 4, the predicted noise spectrum of the wind turbine is presented, along with measured data, in a wind speed of 8 $\mathrm{m\,s^{-1}}$. The simulation was performed assuming a trailing edge (TE) bluntness of 1 % of the chord and a TE angle of 6 °. All

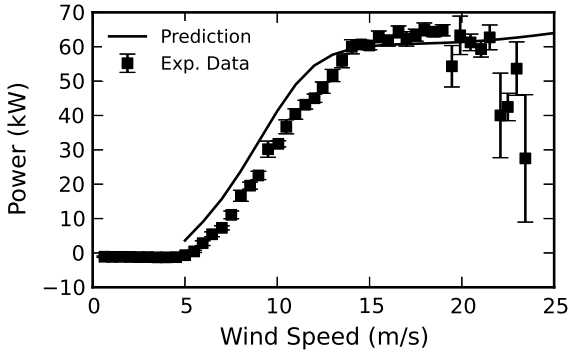

Figure 3: AOC 15/50 predicted and measured power curve (Measurements from Ref. [11]).

noise mechanisms were considered and the observer is located at a position of 32.5 m downwind of the turbine. Besides not being able to predict the peak below 1 kHz and underpredicting the noise levels avove 2 kHz, the prediction tool can be said to provide reasonable results.

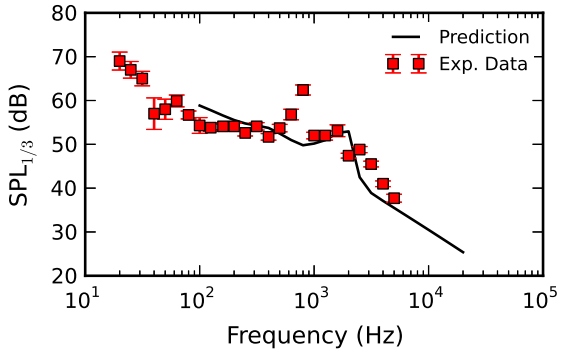

Figure 4: AOC 15/50 overall sound pressure level measurement and prediction data at wind speeds of 8 $\mathrm{m\,s^{-1}}$ (Measurements from Ref. [10]).

4. Results

In this section, the results of the optimizations performed on the NREL Phase II and AOC 15/50 wind turbines are presented and discussed.

All optimizations were performed assuming a wind distribution represented by a Weibull curve with the parameters A and k of 6.48 $\mathrm{m\,s^{-1}}$ and 1.99, respectively, corresponding to an average wind speed of 6.11 $\mathrm{m\,s^{-1}}$. These parameters represent the wind distribution in the Portuguese municipality of Vila do Bispo, in the southwest of Portugal [4].

The performance of the turbine was predicted for a wind speed range from 4 to 25 $\mathrm{m\,s^{-1}}$, in 1 $\mathrm{m\,s^{-1}}$ intervals. Due to this, the noise was predicted for a wind speed of 6 $\mathrm{m\,s^{-1}}$, as it is the closest to the average wind speed of the selected site. A ground roughness value of 0.08 m was chosen. The boundary layer parameters were computed using XFOIL.

4.1. Optimization of the NREL Phase II WT Blade

The Phase II is a three bladed wind turbine developed in NREL for testing purposes. Each blade has a radius of 5.03 m, a hub radius of 0.28 m, uses the S809 airfoil with a constant chord of 0.452 m, and has no twist.

Case 1: Chord and twist SO optimization The first optimization case presented is the Single Objective (SO) optimization of both the chord and the twist of the blade. The chord was defined linearly along the blade with two control points and the twist with a 5^{th} order Bézier curve, leading to a total of 8 design variables.

The AEP was used as the objective function to be maximized and the following constraints were applied:

Chord and Twist Both chord and twist were constrained so that there was a reduction of their values towards the tip of the blade:

$$\begin{aligned} x_i^{cp} &\leq x_{i+1}^{cp} \\ y_i^{cp} &\geq y_{i+1}^{cp} \end{aligned} \tag{11}$$

The optimization resulted in a increase of the AEP up to 46.98 MW h, as summarized in Tab. 1.

Case 2: Chord and twist MO optimization This optimization case consisted in the Multiple Objective (MO) optimization of the problem described in case 1. In order to do so, the OASPL was also used as an objective function, where its minimization was desired.

The initial and final populations of case 2 are presented in Fig. 5, where it can be seen that the optimizer was able to obtain an optimal set of solutions starting from a disperse set. The Pareto front obtained is shown in detail in Fig. 6.

It is visible from that figure that a reduction of almost 2 dB(A) is possible, with no reduction in performance. On the other hand, maintaining the same noise level, an increase in AEP of 20 MW h can be achieved. It is also visible from Fig. 6 that the reduction of noise levels can be achieved between certain ranges of OASPL while maintaining almost the same energy production.

Case 3: Airfoil Shape SO Optimization In this case, the only design variables were the points controlling the airfoil shape in two sections of the blade, at the root hub and tip positions. The only objective function was, like in case 1, the AEP.

The search space of the design variables was defined around the initial airfoil shape variables with

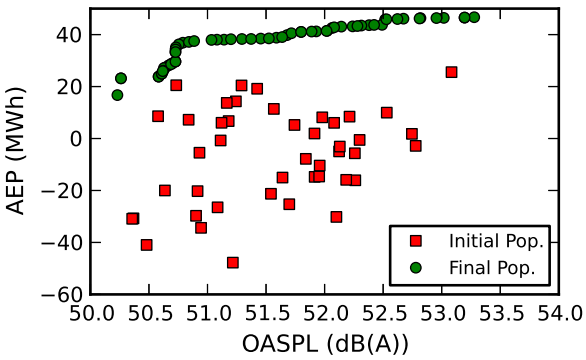

Figure 5: Initial and final populations in case 2.

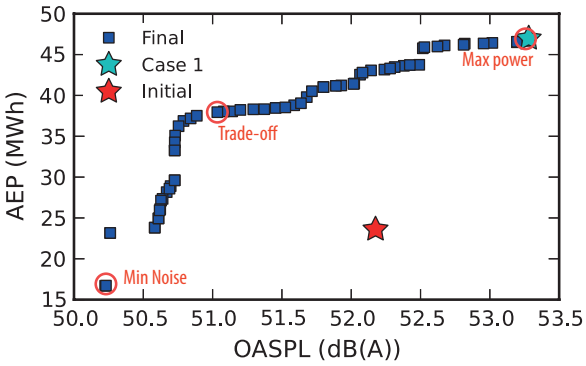

Figure 6: Pareto front in optimization case 2.

a range of ±10% the initial value. The number of design variables at each control section is 20, leading to a total of 40 design variables.

The following constraints were used in this optimization case, in order to guarantee the representation of realistic shapes by the NURBS parameterization.

Control Sections

$$\begin{aligned} x_i^{cp} &\geq x_{i+1}^{cp}, \quad \text{upper curve} \\ x_i^{cp} &\leq x_{i+1}^{cp}, \quad \text{lower curve} \end{aligned} \tag{12}$$

The optimization resulted in an AEP value of 39.22 MW h, as summarized in Tab. 1.

Case 4: Airfoil Shape MO Optimization The multi-objective optimization of the blade, regarding the airfoil shape resulted in the Pareto front presented in Fig. 7. Like in the Pareto front obtained in case 2, this front shows a range of possible solutions where the noise levels can be reduced with only a small decrease in energy production.

In Fig. 8, the three blade geometries corresponding to the solutions highlighted in Fig. 7 are presented with the contour plot of the radial distribution of generated noise levels. There is an evident reduction in the noise levels in the outer region of the blade.

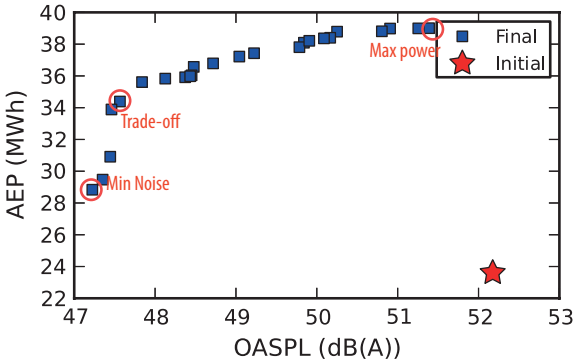

Figure 7: Pareto front in optimization case 4.

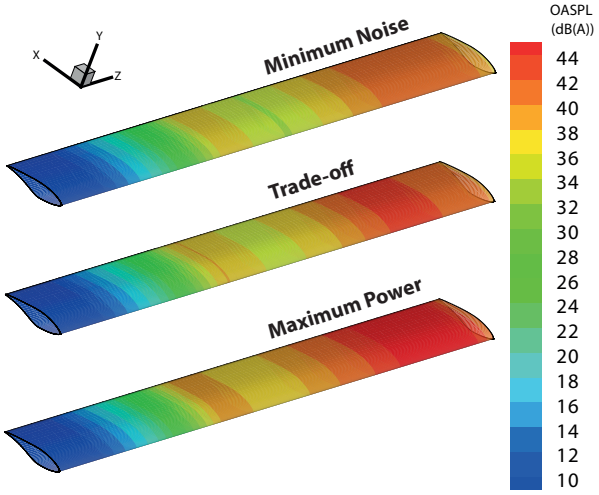

Figure 8: Comparison of the radial distribution of generated noise on between various optimized blades in case 4.

Case 5: Chord, twist and airfoil shape optimization The last optimization case performed on the NREL Phase II wind turbine blade optimized both chord, twist and airfoil shape distributions with both AEP and OASPL as objective functions. The constraints were the same as the previous optimization cases:

Chord and Twist Both chord and twist were constrained so that there was a reduction of their values towards the tip of the blade:

$$\begin{aligned} x_i^{cp} &\leq x_{i+1}^{cp} \\ y_i^{cp} &\geq y_{i+1}^{cp} \end{aligned} \tag{13}$$

Control Sections

$$\begin{aligned} x_i^{cp} &\geq x_{i+1}^{cp}, \quad \text{upper curve} \\ x_i^{cp} &\leq x_{i+1}^{cp}, \quad \text{lower curve} \end{aligned} \tag{14}$$

The Pareto front of this case is presented in detail in Fig. 9, where it can be seen that all optimized

blade geometries result in a reduction of the predicted noise level. It is also visible that a reduction from 50 to 48 dB(A) can be achieved with almost no variation in energy production.

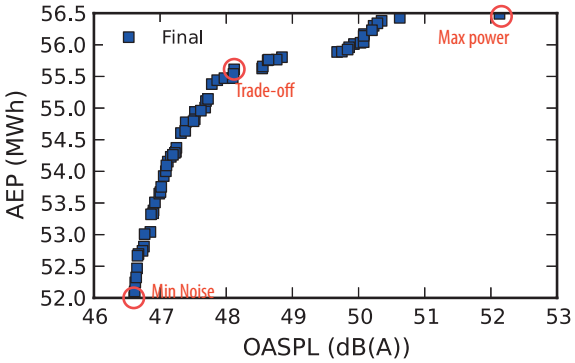

Figure 9: Pareto front in optimization case 5.

The chord and twist distributions of the three different optimized blades are presented in Fig. 10 and Fig. 11, respectively. The three solutions (see Fig. 9) were chosen similarly to the ones in the previous cases (the one generating the minimum noise, the one maximizing energy production and a solution in between the previous two.

Regarding the chord distribution, the three solutions are very similar, with a chord practically constant and equal to the upper limit of 0.754 m along the blade. Although the maximum power blade presents a slightly higher reduction of chord towards the tip, it is only of about 4 cm.

The twist distribution is similar to the ones obtained in the previous cases and the three solutions are very similar between them.

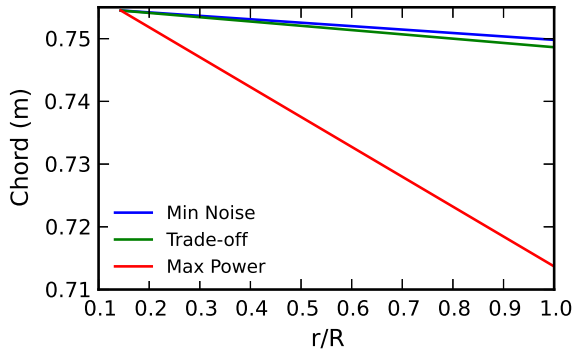

Figure 10: Chord distributions of optimized blades in case 5.

The initial and optimized airfoil shapes at the root and tip positions are shown in Fig. 12 and Fig. 13, respectively. Similarly to the shapes obtained in the previous cases, there is a slightly more accentuated s-tail in the optimized airfoils. In the root region, the three airfoils are very similar to each other, with

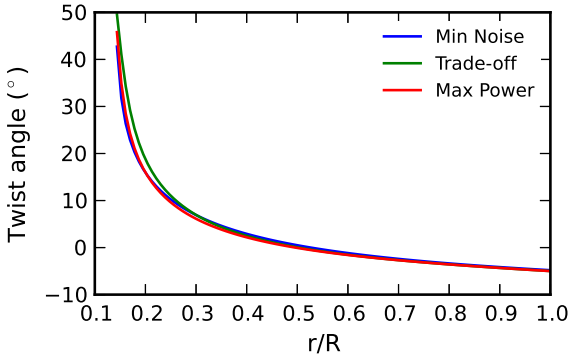

Figure 11: Twist distributions of optimized blades in case 5.

the exception of the upper side of the minimum noise airfoil. At the tip, the differences between the airfoils are more visible, with the trade-off airfoil having a lower curve similar to the maximum power airfoil and an upper curve similar to the minimum noise one.

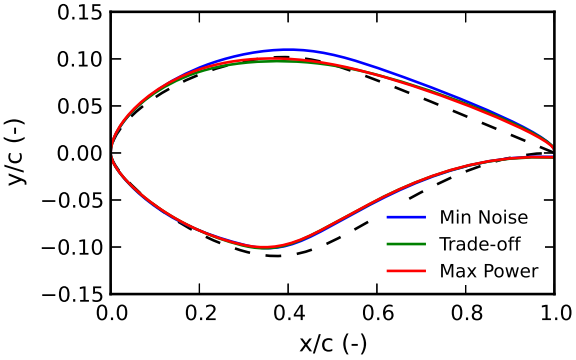

Figure 12: Initial and optimized airfoil shapes at the root in optimization case 5.

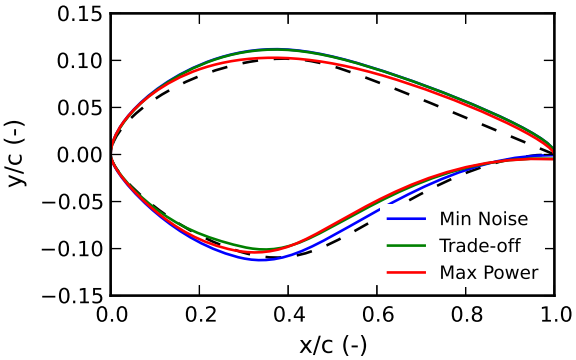

Figure 13: Initial and optimized airfoil shapes at the tip, obtained in optimization case 5.

Figure 14 presents the noise field generated by each of the three optimized blades, where it can be seen that higher noise levels are generated when

the blade is descending. By comparing the three solutions, it can be seen that the maximum power solution presents much higher noise values than the other two and that the reduction in noise from one solution to another happens mostly in the outer part of the blade.

Summary of NREL Phase II optimization results The summary of the AEP and OASPL values obtained in all the previous described optimization cases are presented in Tab. 1, where it can be seen that with increasing number of variables used in the problem, the optimal solutions presents lower noise levels and higher energy production levels.

Case		AEP [MW h]	OASPL [dB(A)]
	Initial	23.6	52.18
1		46.98	53.28
2	**Min. Noise**	16.7	50.22
	Trade-off	38.04	51.08
	Max. Power	46.74	52.28
3		39.22	52.11
4	**Min. Noise**	28.83	47.22
	Trade-off	35.61	47.84
	Max. Power	39.01	51.38
5	**Min. Noise**	52.01	46.61
	Trade-off	55.54	48.11
	Max. Power	56.49	52.13

Table 1: Summary of the optimization cases performed on the NREL Phase II wind turbine blade.

4.2. Optimization of the AOC 15/50 wind turbine blade

Due to the simplicity of the NREL Phase II blade, high aeroacoustic improvements were expected to be achieved. The results showed that reduction in noise levels is possible without much, if any, reduction in aerodynamic performance. The previous results also showed that if not properly constrained, the solution might converge to geometries that might have unwanted structural characteristics. With this in mind, an optimization was performed on the AOC 15/50 turbine blade and is presented in this section.

Design Variables The AOC 15/50 airfoil shape is defined at 4 stations, being the first at the hub considered to be circular. At each control section, the coordinates of 10 control points were used as design variables (the same as in the previous optimization cases minus the y-coordinates of control points 0 and 12), resulting in 54 variables (18 per control section). The twist was defined using a 5^{th} order Bézier curve,

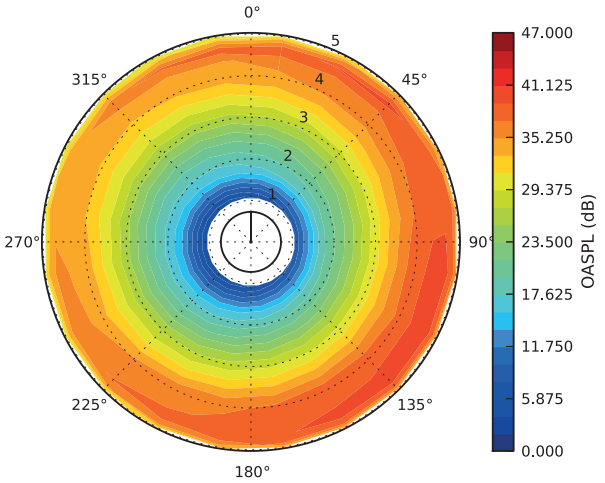

(a) Min. Noise

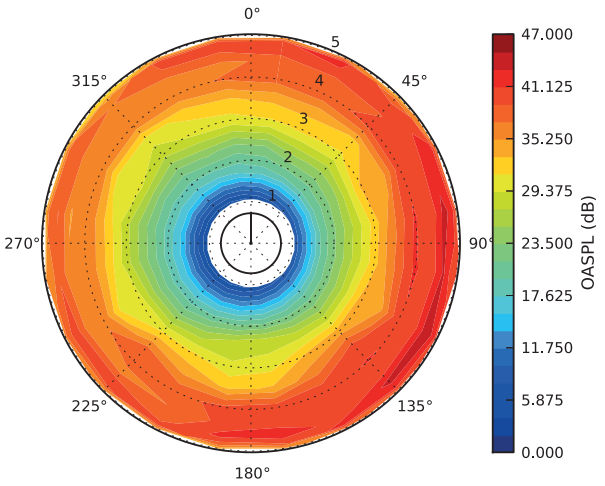

(b) Trade-off

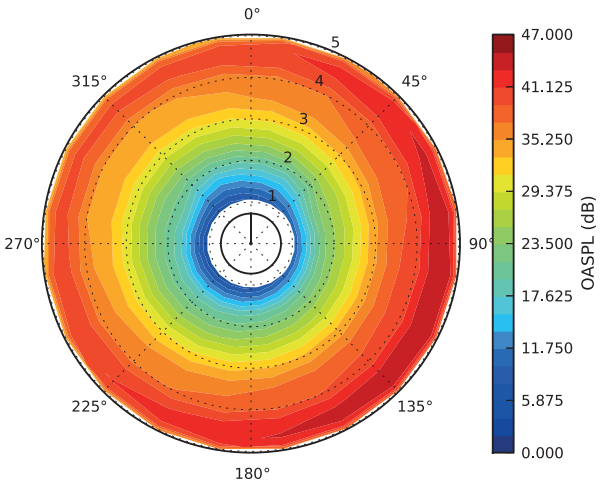

(c) Max. Power

Figure 14: Overall sound pressure level across the rotor for various optimized blades from case 5.

resulting in 6 design variables. The chord defined by linear interpolation of 3 control points, resulting in 2 design variables. The search space of the con-

trol section variables was defined as ±10% in the x-direction and ±20% in the y-direction, relative to the initial control points. The chord variables search space was defined as ±20% of the initial chord values and the twist as ±30% in the x-direction and and ±10% in the y-direction. This resulted in a total of 62 design variables.

The constraints used in this optimization case were the following:

Chord and Twist Both chord and twist were constrained so that there was a reduction of their values towards the tip of the blade (not counting with the chord at the root):

$$\begin{aligned} x_i^{cp} &\leq x_{i+1}^{cp} \\ y_i^{cp} &\geq y_{i+1}^{cp} \end{aligned} \tag{15}$$

Control Sections

$$\begin{aligned} x_i^{cp} &\geq x_{i+1}^{cp}, \quad \text{upper curve} \\ x_i^{cp} &\leq x_{i+1}^{cp}, \quad \text{lower curve} \\ y_2^{cp} &\geq y_3^{cp} \\ y_{10}^{cp} &\geq y_9^{cp} \end{aligned} \tag{16}$$

Run Conditions The TE thickness was assumed to be 1% of the chord, with a constant angle of 6 %. Due to the non aerodynamic shape of the sections up to 40 % of the blade, the noise was only computed in the 60% outer part.

Results The resulting Pareto front is presented in Fig. 15 where three solutions are identified, similarly the previous optimization cases. A reduction in OASPL of more than 4 dB(A) is possible, relative to the initial blade, without any loss in energy production. On the other hand, while maintaining the noise levels, an increase of 14 MW h can be achieved. The Pareto front ranges between an OASPL of 56 dB(A) to about 63 dB(A) and from about 57.5 dB(A) to 63 dB(A) the AEP varies very little. The AEP and OASPL values of the initial blade and the three solutions identified in Fig. 15 are presented in Tab. 2.

Figures 16 and 17 present the chord twist distributions, respectively, of the three solutions indicated in Fig. 15. The chord was maximized to the upper bounds at 0.4 and 1.0 r/R in the three solutions, with the exception of the minimum noise solution, where the chord is slightly smaller than the other solutions at 0.4 r/R. Regarding the twist distributions, the three solutions present higher twist angles than the initial values allover the blade, with the exception of the tip region, where the twist change rate increases and the twist angles are lower than the initial values.

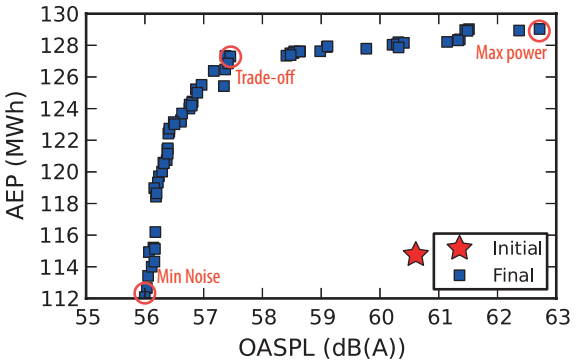

Figure 15: Pareto front in AOC 15/50 blade optimization case.

	AEP [MW h]	Difference [%]	OASPL [dB(A)]	Difference [%]
Initial	114.76	0	60.61	0
Min. Noise	112.09	- 2.3	56	- 7.6
Trade-off	127.33	11.0	57.37	- 5.3
Max. Power	129.03	12.4	62.72	3.5

Table 2: Summary of AEP and OASPL values in AOC 15/50 optimization case.

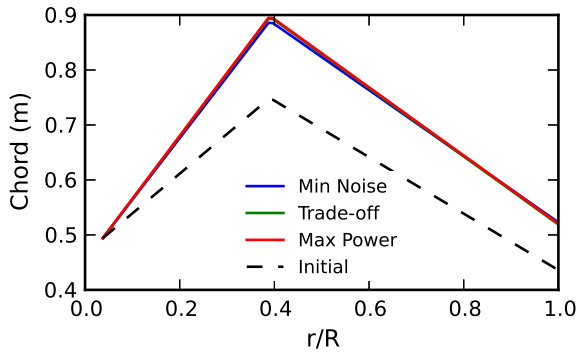

Figure 16: Chord distributions of optimized AOC 15/50 blades.

The airfoil shapes of the three solutions are presented in Figures 18 to 20. The same behavior of previous cases is observed in these results regarding the differences between the airfoil shapes of the different solutions. While at 40% and 75% of the blade, the Trade-off airfoil shape is a mixture of the other two, at 95% of the blade it is much closer to the Minimum Noise airfoil shape, particularlly the upper side. This comes as a result of the previously mentioned fact that the noise is mainly generated

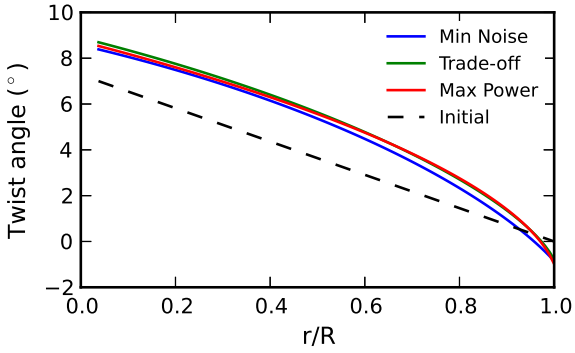

Figure 17: Twist distributions of optimized AOC 15/50 blades.

in the outer region of the blade.

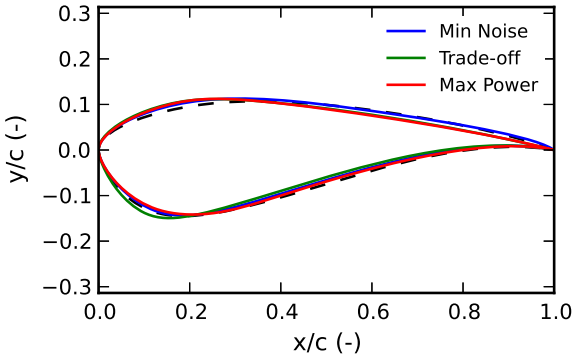

Figure 18: Initial and optimized airfoil shapes at 40% of the blade in the AOC 15/50 blade optimization

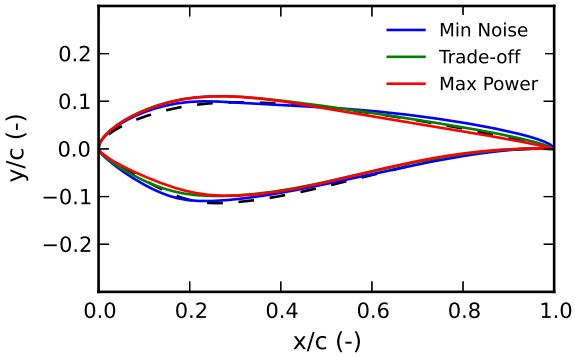

Figure 19: Initial and optimized airfoil shapes at 75% of the blade in the AOC 15/50 blade optimization

The three solutions are also compared in Fig. 21, where the radial distribution of generated noise in each optimized blade is presented. It can be seen from that figure that the reduction of noise from the maximum power solution to the minimum noise occurs specially in the outer part of the blade.

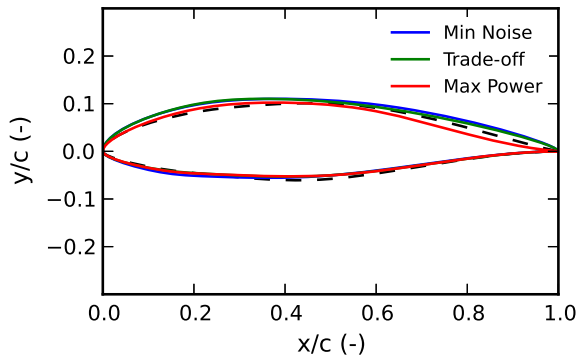

Figure 20: Initial and optimized airfoil shapes at 95% of the blade in the AOC 15/50 blade optimization

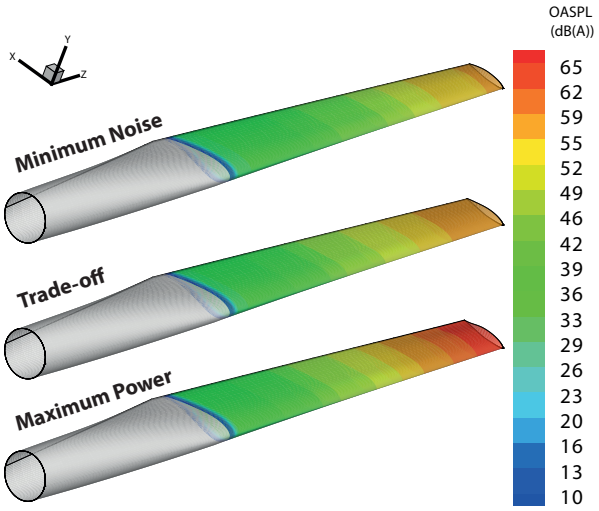

Figure 21: Comparison of the radial distribution of generated noise on between different optimized AOC 15/50 blade geometries.

5. Conclusions

In the present work, a wind turbine aerodynamic and aeroacoustic prediction model was successfully implemented and validated against experimental data.

A geometrical model of the wind turbine blade was also developed and implemented, using NURBS curves and Bezier curves, for the definition of the cross sectional airfoil shapes and twist and chord distributions, respectively. The NURBS parameterization of the airfoil shapes proved to be able to reproduce various different airfoil shapes commonly used in wind turbines.

The code was successfully implemented into an optimization framework, being able to produce optimal solutions in the various performed test cases. In the optimizations performed on the NREL Phase II wind turbine, a maximum increase in AEP of 139.4 % and maximum reduction of OASPL in 10.7 % was achieved. These large relative improvements showed

that this particular blade was far from being optimal. In contrast, using another blade, from the commercially available AOC 15/50 wind turbine, it was possible to assess more realistically the potential of the optimization framework. In this case, the optimization resulted in a maximum improvement in AEP of 12.4 % and a maximum OASPL reduction of 7.6 %. However, these results were not achieved in the same blade geometry, and the trade-off between noise generation and energy production is visible in the results of the optimizations.

Nowadays, tools like the framework developed are used in the design phase of any wind turbine to increase its performance to the maximum possible extent. As the geometries of the blades are already highly manually tuned by the designers, the use of such tools might give the wind turbine a competitive edge. The relative small computational requirement of each optimization is a key factor, as it allows for a greater diversity of geometries and configurations to be analyzed / optimized, thus increasing the probability of obtaining a better solution.

Acknowledgements
The author would like to thank Dr. André Calado Marta for his teachings guidance throughout the development of this thesis.

References

[1] R. Amiet. Acoustic radiation from an airfoil in a turbulent stream. *Journal of Sound and Vibration*, 41(4):407–420, 1975.

[2] T. Brooks, D. Pope, and M. Marcolini. *Airfoil self-noise and prediction*, volume 1218. National Aeronautics and Space Administration, USA, 1989.

[3] W. Colby, R. Dobie, G. Leventhall, D. Lipscomb, R. McCunney, M. Seilo, and B. Søndergaard. *Wind turbine sound and health effects: An expert panel review.* American Wind Energy Association, 2009.

[4] P. Costa. Atlas do potencial eólico para Portugal continental. Master's thesis, Faculdade de Ciências da Universidade de Lisboa, Lisboa, 2004.

[5] K. Deb, A. Pratap, S. Agarwal, and T. Meyarivan. A fast and elitist multiobjective genetic algorithm: Nsga-ii. *Evolutionary Computation, IEEE Transactions on*, 6(2):182–197, 2002.

[6] M. Drela. XFOIL - An analysis and design system for low Reynolds number airfoils. *Low Reynolds number aerodynamics*, 5-7 June 1989.

[7] Z. Du and M. Selig. A 3-d stall-delay model for horizontal axis wind turbine performance prediction. In *Proceedings of the 1998 ASME Wind Energy Symposium, Reno, NV*, pages 9–19, 1998.

[8] A. Eggers, K. Chaney, and R. Digumarthi. An assessment of approximate modeling of aerodynamic loads on the UAE rotor. ASME, 2003.

[9] M. Hansen. *Aerodynamics of wind turbines.* Earthscan, London Sterling, VA, 2008.

[10] A. Huskey, H. Link, and C. Butterfield. Wind turbine generator system acoustic noise test report for the aoc 15/50 wind turbine. Technical report, AOC1550-CA-99182-1000, National Renewable Energy Laboratory, Golden, CO, 1999.

[11] R. Jacobson, E. Meadors, and H. Link. Power performance test report for the aoc 15/50 wind turbine, test b in golden, colorado. *United States Department of Energy by National Wind Technology Centre. National Renewable Energy Laboratory*, pages 1–150, 2003.

[12] M. Lowson. *Assessment and Prediction of Wind Turbine Noise.* Energy Technology Support Unit, 1993.

[13] P. Moriarty, G. Guidati, and P. Migliore. Recent improvement of a semi-empirical aeroacoustic prediction code for wind turbines. In *Proc., 10^{th} AIAA/CEAS Aeroacoustics Conference, Manchester, UK*, 2004.

[14] P. Moriarty, G. Guidati, and P. Migliore. Prediction of turbulent inflow and trailing-edge noise for wind turbines. In *11^{th} AIAA/CEAS Aeroacoustics Conference(26^{th} Aeroacoustics Conference)*, pages 1–16, 2005.

[15] R. E. Perez, P. W. Jansen, and J. R. R. A. Martins. pyOpt: A Python-based object-oriented framework for nonlinear constrained optimization. *Structures and Multidisciplinary Optimization*, 45(1):101–118, 2012.

[16] L. Viterna and D. Janetzke. *Theoretical and experimental power from large horizontal-axis wind turbines.* U.S. Department of Energy, Conservation and Renewable Energy, Wind Energy Technology Division, 1982.

[17] S. Wagner, R. Bareiss, and G. Guidati. *Wind turbine noise.* Springer, Berlin, 1996.